Analyst

Accepted Manuscript

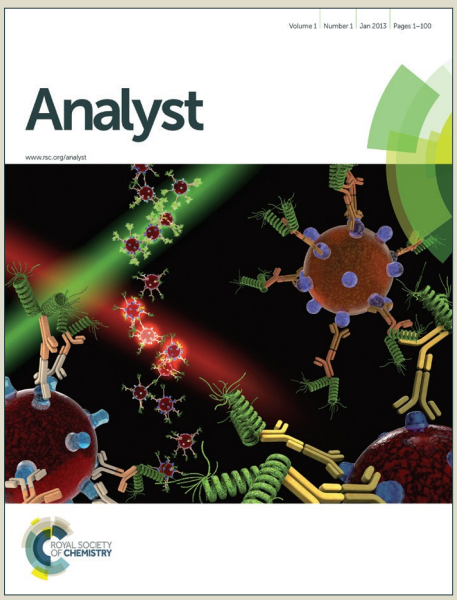

ROYAL SOCIETY OF CHEMISTRY

www.rsc.org/analyst

Contribution of Raman spectroscopy in nephrology: a candidate technique to detect hydroxyethyl starch of third generation in osmotic renal lesions

Figure Legends

Figure 1: Raman spectra of starch (black) and HES 130/0.4 (red). The highest intensity peak is identified at 480 cm^{-1} in both spectra.

Figure 2: Principal Component Analysis (PCA) of Raman spectra of HES-incubated and sham monocytes. The score plot on the two first components shows a clear spectral discrimination of the HES-incubated and sham monocytes along PC1 (A). The first principal component (PC1) presents a high intensity region around 480 cm^{-1} (B).

Figure 3: Masson trichrome staining showing osmotic nephrosis injuries with vacuolated tubular cells (star) side by side with normal tubular sections (triangle)(x40) (A). Photo of a 10µm-thick frozen slide of the same renal biopsy dedicated to Raman acquisition, tubular sections with vacuolated cells cannot be detected on this photograph (B). (Scale bars: 25 µm)

Figure 4: Analysis by Raman spectroscopy of kidney biopsy with osmotic nephrosis lesions associated with HES 130/0.4. A spectral difference at the level of the vibration around 480 cm^{-1} is clearly visible between the two representative spectra as displayed in the inserts. (Scale bar: 25µm)

Panel A: Spectral image from case#2 built by intensity ratio (480/1660 cm^{-1}). Tubular sections are outlined with a dotted line. The color scale represents the intensity ratio: from violet (ratio=0) to red (ratio=1). Red areas on certain tubular sections can be highlighted while adjacent tubular sections appeared in violet or blue. Panel B: Raman spectra extracted from two points of the spectral image, corresponding to the blue area (♦) and red area (*).

Figure 5: Spectral images from the four cases: #1 (A) #2 (B) #3 (C) #4 5(D) and from a negative control (E). Spectral images from cases (A to D) present high intensity ratio while the negative control spectral image (E) is only composed of pixels with low intensity ratio similarly to other negative controls. (Scale bars 50µm)

Figure 1

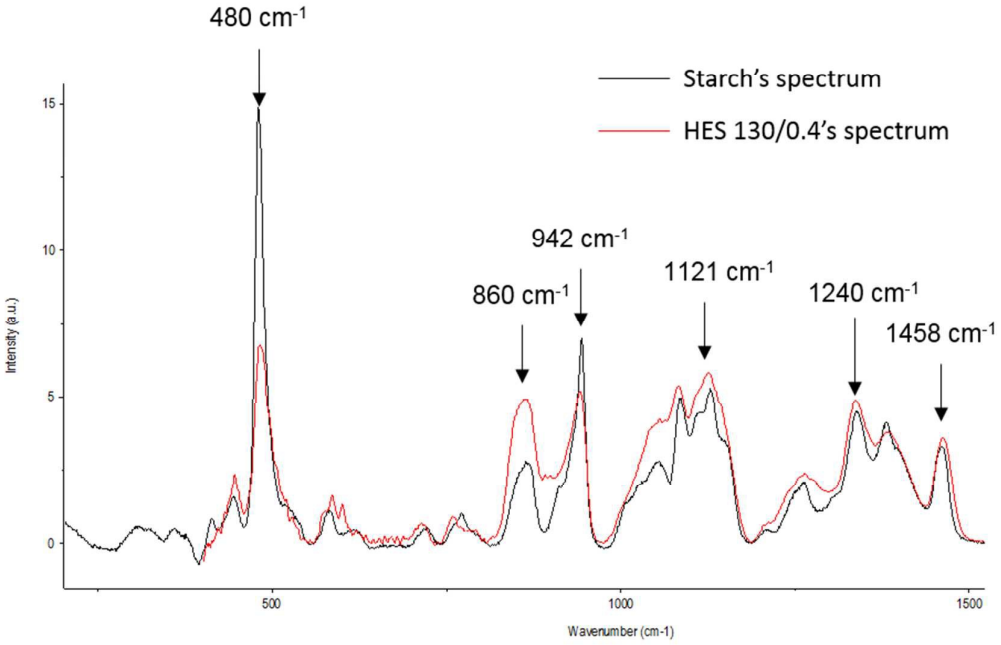

Figure 2

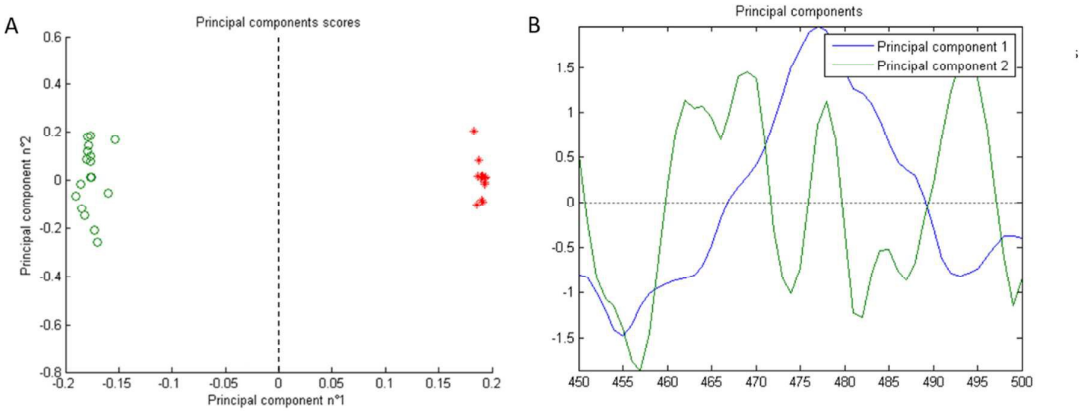

Figure 3

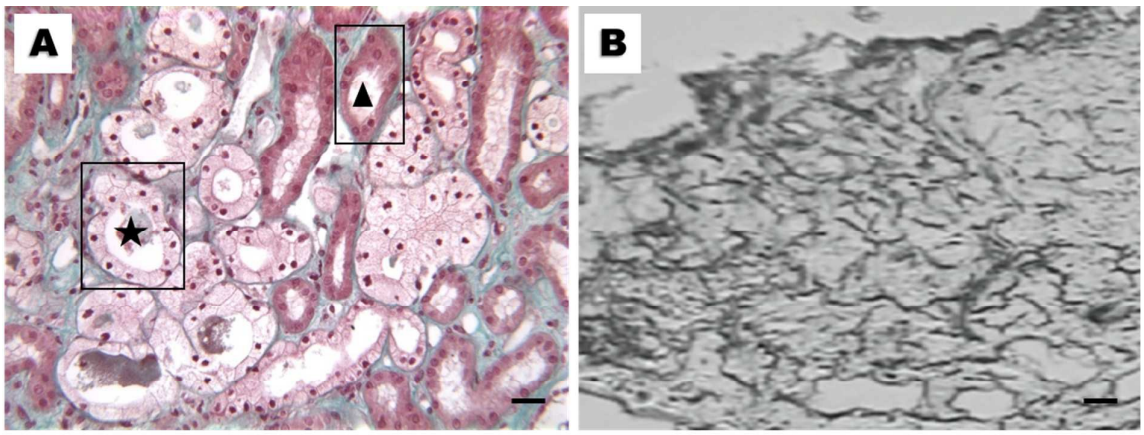

▲ Normal tubular section

★ Tubular section with osmotic-nephrosis lesion

Figure 4

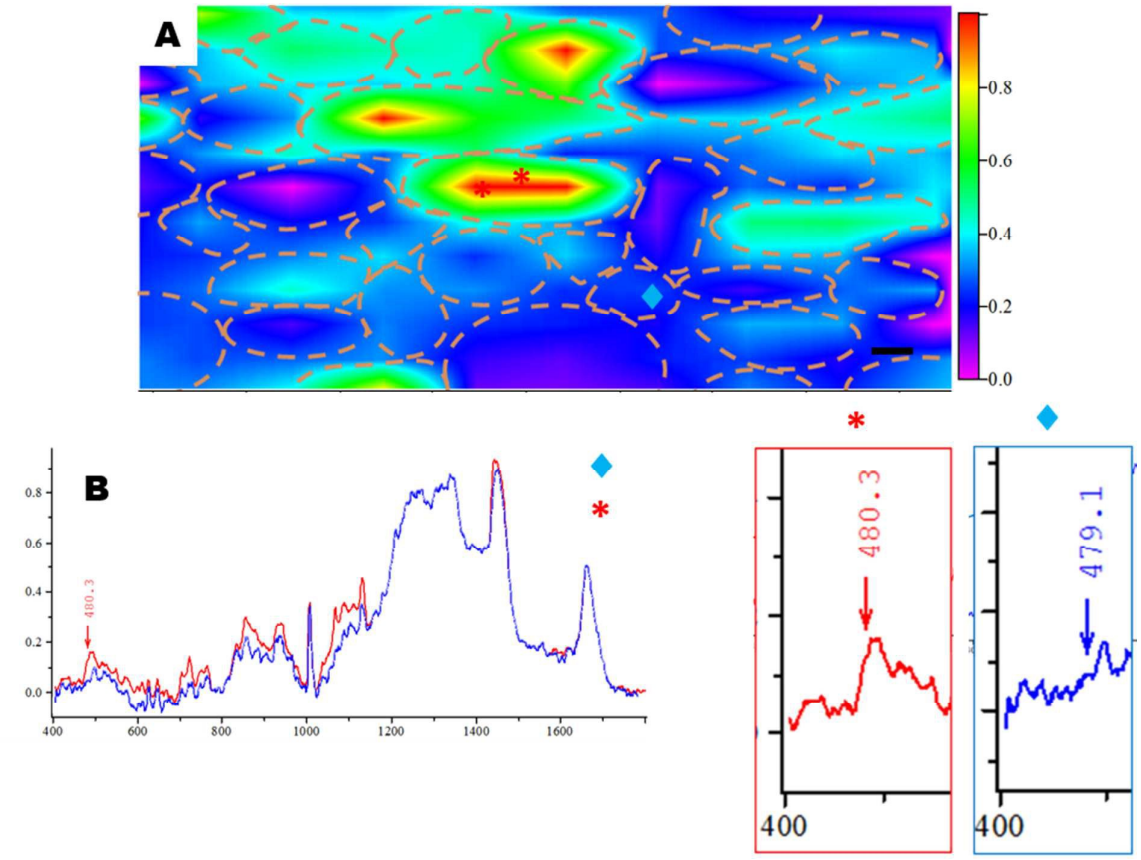

Figure 5

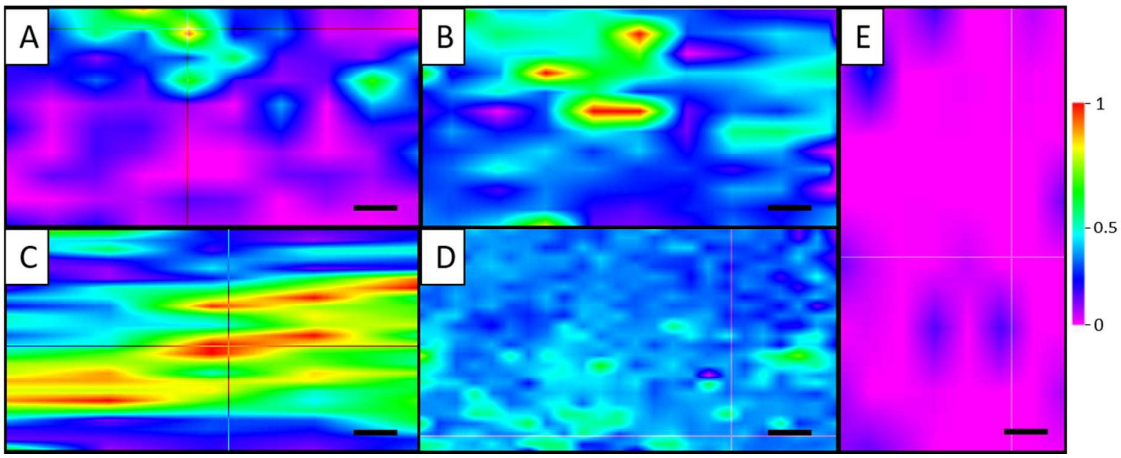

Raman Spectroscopy, a candidate tool for drug detection in kidney: case of HES, a volume expander administrated after hemodynamic instability

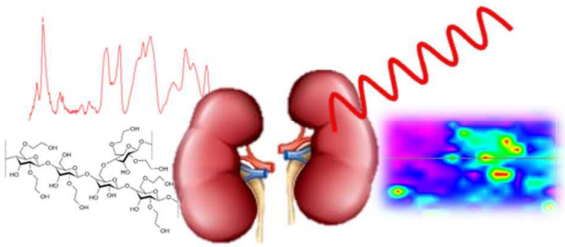

Contribution of Raman spectroscopy in nephrology: a candidate technique to detect hydroxyethyl starch of third generation in osmotic renal lesions

V. Vuiblet [1,2,3] ; T.T. Nguyen [1]; A. Wynckel [2]; M. Fere[1] ; L. Van-Gulick[1]; V Untereiner[1] P. Birembaut [3]; P. Rieu [1,2] and O. Piot [1,4]

[1] UMR CNRS 7369 MEDyC, Université de Reims Champagne- Ardenne, Reims, France

[2] Nephrology division, Maison Blanche University Hospital, Reims, France

[3] Histology Laboratory Pol Bouin, Maison Blanche University Hospital, Reims, France

[4] PICT (Cellular and Tissular Imaging Platform), Université de Reims Champagne-Ardenne, Reims, France

Key Words: HydroxyEthyl Starch; Kidney; Osmotic Nephrosis; Raman spectroscopy.

Short title: HES detection in kidney by Raman microscopy

Address for correspondence : Vincent Vuiblet

Service de Néphrologie et de Transplantation, Centre Hospitalier et Universitaire

45 rue Cognacq-Jay, 51092 Reims, France

Tel : (33) 326787632 Fax : (33) 326783776

Email : vvuiblet@chu-reims.fr

Abstract

Background and objectives: HydroxyEthyl Starch (HES) has been one of the most commonly used colloid volume expanders in intensive care units for over 50 years. First and second generation HES, with a high molecular weight (≥200 kD) and a high degree of substitution (≥ 0.5), has been associated with both renal dysfunction and osmotic nephrosis-like lesions on histological studies. Recently, third generation HES (130 kD/ < 0.5) has also been shown to impair renal function in critically ill adult patients although tubular accumulation of HES has never been proven in the human kidney. Our objective was to demonstrate the potential of Raman micro-imaging to bring out the presence of third generation-HES in kidney of patients having received the volume expander. **Design:** Four biopsies presenting osmotic nephrosis-like lesions originated from HES-administrated patients with impaired renal function were compared to HES-negative biopsies (n=10) by Raman microspectroscopy. **Results:** The first step was dedicated to the identification of a specific vibration of HES permitting to detect the cellular and tissular accumulation of the product. This specific vibration at 480 cm^{-1} is assigned to a collective mode of the macromolecule; it is located in a spectral region with a limited contribution from biological material. Based on this finding, HES distribution within tissue sections was investigated using Raman micro-imaging. Determination of HES positive pixels permitted clearly to distinguish positive cases from HES-free biopsies (proportions of positive pixels from the total number of pixels: 23.48% ± 28 vs 0.87% ± 1.2; p=0.004). **Conclusions:** This study shows that Raman spectroscopy is a candidate technique to detect HES in kidney tissues samples currently manipulated in nephrology departments. In addition, on the clinical aspect, our approach suggests that renal impairment related to third generation HES administration is associated with osmotic nephrosis-like lesions and HES accumulation in the kidney.

Introduction

Critical illness such as severe sepsis or septic shock, is a common cause of acute kidney injury (AKI) [1], which is associated with worse prognosis [2]. Management of collapse includes fluid resuscitation therapy by aggressive filling, which appears to be essential to reduce mortality [3]. Quick restoration of hemodynamic conditions is crucial to limit renal injury.

Hydroxyethyl starches (HES) are commonly used colloid volume expanders that have been used in intensive care units for over 50 years. HES are heterogeneous molecules that are produced by hydrolysis and hydroxyethylation of amylopectin, a highly branched starch that is obtained from waxy maize or potatoes. Natural starches cannot be used as plasma substitutes because they are unstable and are rapidly hydrolyzed by circulating amylase. Substituting hydroxyethyl for the hydroxyl groups on glucose molecules increases solubility and delays hydrolysis of the compound by amylase, thereby delaying its breakdown and elimination from the blood. Glucose molecules are substituted at the C2, C3 and C6 positions. HES preparations with a higher molecular weight, degree of substitution and substitution ratio at C2/C6 have slower metabolism and elimination. Early forms of this solution had a high molecular weight (200 kd) and a high degree of substitution (0.5 or 0.6), and were associated with both renal dysfunction and increased risk of bleeding[4-6]. Some histological studies have shown morphological abnormalities of the proximal tubular epithelial cells after infusion of HES 200/0.5 (“osmotic nephrosis-like injuries”), probably reflecting the accumulation of proximal tubular lysosomes due to pinocytosis of exogenous osmotic solutes [7].

A “third-generation” HES (HES 130/<0.5) has been developed that has a lower molecular weight (130 kd) and a lower degree of substitution (<0.5). This new form

purports not to induce renal injury thanks to these characteristics. However, recent observational studies and randomized controlled trials comparing HES 130/<0.5 with crystalloid solution reported increased mortality and severe renal injury with the use of HES 130/<0.5 in critically ill adult patients, including patients with sepsis, and patients admitted to intensive care [8-10]. In November 2013, the U.S. Food and Drug Administration (FDA) has concluded a boxed warning on increased mortality and severe renal injury and risk of bleeding. FDA has recommended avoid use of HES solution especially in critically ill adult patients, in patients with pre-existing renal dysfunction and in patients undergoing open heart surgery. [11]

One hypothesis to explain the renal toxicity of HES is the accumulation of macromolecules in renal tubular cells, where they cannot be degraded because of their physicochemical properties[12]. However, while the presence of HES has been detected by immunohistochemistry in several tissues (skin, liver, spleen, intestine, and muscle) [12, 13], tubular accumulation of HES has never been demonstrated in the human kidney.

Raman spectroscopy (RS) is a photonic technique based on the inelastic scattering of light generated by the interaction of a monochromatic radiation with a sample. The spectral analysis of the scattered light gives access to the vibrational modes of the molecular constituents of this sample [14]. In addition to the high molecular specificity, RS presents the advantages to be non-invasive and non-destructive, what is of interest in biology and medicine [15]. Moreover, unlike conventional biological assays, analysis of tissues with RS does not require the use of fixatives, markers or stains. The coupling of a Raman spectrometer with an optical microscope, makes it possible to collect spectra from volumes of the order of 1 μm^3, enabling the analysis of microscopic features of biological samples. In pharmaceutical research, RS permits to characterize drugs and their behavior in biological models [16] (Specific spectral

signatures of molecules make it possible to follow release of drugs and pharmacokinetics in cells tissue such as neoplastic cells [17] or in tissues like skin [18-21]. In addition, molecular alterations of tissue associated with a pathological state can be probed by RS. Examples include the detection of cholesterol crystals in atherosclerotic plaques [22], the characterization of steatosis and fibrosis in liver disease [23], or the blood glucose quantification in diabetes [24]. On the basis of this analytical potential, our purpose was to demonstrate the feasibility to use Raman micro-imaging, a specificity-high label-free technique, to detect the tubular accumulation of HES of third generation in kidney biopsies. Previously to the tissue investigation, the methodology was first worked out on monocytes as cellular model because of their ability to incorporate macromolecules such as HES in their lysosome in cytoplasmic compartment by phagocytosis.

Methods

Preparation of monocyte samples

Monocytes were isolated from total human blood by elutriation and placed in BSA-coated cryotubes and were rested overnight at 37°C. Then, cells placed on 4 CaF_2 supports (Crystran, Dorset, UK) (106 cells per supports). A fraction of monocytes was incubated with 100 µL of containing Hank's Balanced Salt Solution (HBSS, Gibco) plus 100 µL of commercial HES solution (Voluven®, Fresenius Kabi) during 24 hours at 37°C. Control negative cells placed on 2 CaF_2 supports (106 cells per support), were incubated with 100 µL of containing Hank's Balanced Salt Solution (HBSS, Gibco) plus 100µL of 0.9% saline solution during 24 hours at 37°C.

After incubation, adherents cells were washed with 0.9% saline solution four time and then were dry fixed overnight before analysis.

Each support was analyzed by optic microscopy to confirm presence of living cells on CaF_2 supports. Then Raman micro-imagery analysis was performed on each support as described below.

Patients

For the purpose of this study, we selected patients who: (1) experienced shock associated with acute renal failure; (2) received HES 130/0.4 solution for fluid resuscitation; (3) had persistent renal failure several weeks after the acute event; (4) were diagnosed to have osmotic nephrosis lesions on a renal biopsy. Four patients hospitalized in our nephrology division met criteria for the study. Clinical and laboratory information was obtained from medical records of these patients. Main clinical data of these patients are summarized in Table 1.

Controls

The negative control group included 10 renal biopsies from 10 patients who never received HES. This group of biopsies comprised intravenous immunoglobulin-induced osmotic nephrosis-like lesions, two diabetic nephropathies, one chronic tubulo-interstitial nephropathy, one amyloid light-chain (AL) amyloidosis, one myeloma tubulopathy without amyloidosis, one oxalosis, one biopsy with tubular cell vacuolizations associated with calcineurin inhibitor toxicity, and two normal renal biopsies.

Histopathological Assessment

Renal biopsies were fixed in Dubosq-Brazil and dehydrated then paraffin-embedded. Two-µm sections were deposited on Superfrost 2® slides and stained with Masson trichrome. This precision was added in the manuscript in the Material and Methods session.

Histological assessment was performed using light microscopy by examination of renal biopsy by pathologists.

Raman acquisition parameters

Raman acquisitions were performed using a LabRam Raman microspectrometer (Horiba Scientific, Villeneuve d'Ascq, France), equipped with a 785 nm near-infrared excitation source delivered by a Titanium-Saphir laser. Interferential and edge filters were integrated to this device to reject parasitic excitation wavelengths and Rayleigh scattering or laser reflection respectively. The analysis of the Raman signals was carried out using holographic dispersive grating (950 g/mm) and a CCD (Charge Coupled Device) camera permitting to measure simultaneously several wavelengths in one shot. Thus, spectral data were collected on a spectral range from 400 to 1780 cm^{-1}, with a spectral resolution of 4 cm^{-1}. The spectrometer was coupled with an optical upright microscope (Olympus®, Bx40) equipped with a 100X objective either water immersion for HES solution analysis (NA=1, LumPlan, Olympus®), or dry objective for cells and tissue measurements (NA = 0.9, MPlan, Olympus®). The laser power at the objective output was measured to 30 mW. Samples to be analyzed were deposited on CaF_2 substrates (Crystran, Dorset, UK) appropriate for near infrared Raman spectroscopy.

Acquisition parameters were controlled by Labspec® software (Horiba Scientific). This software also makes it possible to process spectra in order to reduce noise by smoothing, to correct baseline drift or to normalize data.

Cells Raman Analysis

Acquisitions of spectral point were focused on cytoplasmic compartment, which corresponds to preferential cell accumulation sector of HES phagocytosis. Spectra were collected with an acquisition time of 45 s repeated thrice

Spectral image acquisition on kidney biopsies

For renal tissue analysis, Raman images were collected by means of a XY motorized stage. Ten µm-thick sections were cut from frozen biopsies by using a cryomicrotome. Regions of interest selected from white light image of the tissue section were mapped using point by point image mode with a lateral displacement step of 1 µm in both X and Y directions and an acquisition time of 45 s per pixel. In our investigation for both negative controls and positive specimens, tubular section areas of about 500 μm^2 were imaged.

Research of HES specific Raman vibrations

The aim of this preliminary analysis is to determine the vibrations that could be used for the HES detection. For the HES 130/0.4, reference signature spectra of the commercial solution (Voluven®, Fresenius Kabi, Bad Homburg, Germany), of the dehydrated form, and of starch (starch from wheat, Sigma Aldrich, Lyon, France) were collected with an acquisition time of 30 seconds and 3 accumulations per measurement.

Mean Raman spectra of pure starch and HES 130/0.4 are displayed in Figure 1. The two products present quite similar signatures. Table 2 indicates the main vibrations of HES. Interestingly, an intense and sharp signal appears at 480 cm^{-1}, this vibrations assigned to a collective vibration mode of the macromolecule skeleton [25, 26].

Data processing for monocyte spectral analysis

Data were processed by PCA (Principal Component Analysis) which is considered as the reference unsupervised method for spectral data exploration. PCA is commonly used to separate different groups of spectra together with identifying discriminant spectral features between these groups (ref).

PCA was performed on mean-centered spectra on spectral window of interest to detect HES 130/0.4 (470-490 cm^{-1}). Spectra were previously baseline-corrected using polynomial function (degree 5), smoothed using Stavisky-Golay polynomial function (degree 2) and normalized on Amide I band reflecting the total protein content using Labspec software (Horiba Scientific). MATLAB 8.3 software (The Mathworks, USA) was used to run PCA.

Statistical analysis

HES Raman-based quantifications for negative controls and positive specimens were compared with using the Mann-Whitney non-parametric test using SPSS software (v 20.0, IBM Company, Chicago, Ill, USA).

Results

HES-incubated monocytes as simple/plain biological material to identify HES specific Raman marker

Preliminary to tissue investigation, first experiments were carried on monocyte cell culture, in order to compare the Raman signal between monocytes incubated with HES solution and negative control cells incubated with 0.9% saline solution (Fig S1). Spectral data were processed by PCA, which is a standard statistical classification unsupervised method. This statistical approach permitted to consider the variability inherent to the biological specimens. First, a number of 12 components explaining 99% of the variance of the data set was retained. For searching a distinction between

the two groups of spectra, we considered the two first components since they contain the most variance, with 77% and 14% respectively. Score plot with the first and second components as projection axes showed a clear distinction between the two populations of spectra (Fig 2A). Since the scores of the first component (PC1) appeared strongly discriminant, we focused on the signals composing PC1 (Fig 2B). The signal at 480 cm^{-1} can be highlighted confirming the specificity of this vibration for HES detection in biological material. Based on this result, the collective mode vibration of starch appeared as a candidate marker of HES, especially as cells or tissues present low signal intensity in this spectral region (Tab 1).

HES detection in kidney tissue samples

For the analysis of kidney biopsies, we focused our investigation on areas containing tubular sections, identified by light microscopy, since these entities ensure the main reabsorption function in kidney. Contrarily to Masson's trichrome staining (fig 3A), the with light observation way of the Raman device do not allow to verify that the tubular sections contained vacuolated tubules (Fig 3B). An example of Raman image collected on such a tissue region of interest is shown Fig 4; it concerns a biopsy from case #2 that was the most severe case of this study. Indeed, case #2 corresponded to a patient with normal eGFR at baseline and without renal function recovery requiring the pursuit of hemodialysis after septic shock and administration of HES 130/0.4.

The Raman mapping was performed on a 10^3 μm^2 area. In order to recover/visualize the spatial distribution of HES within the tissue, it is necessary to perform a spectral

normalization to avoid possible bias induced by variations in the thickness of tissue slicing or in the material density. Consequently, the amide I band centred around 1656 cm^{-1} and assigned to the total protein component was taken as reference vibration. Thus, HES distribution was visualized by computing the ratio of integrated intensities between the 480 cm^{-1} collective mode of HES [470-490 cm-1] and the Amide I band 1500-1700 cm^{-1}] (Fig 4A). In this case, the distribution was heterogeneous as highlighted by the color-code scale constructed according the 480/Amide I ratio. From this scale and the observation of the reconstructed chemical Raman image, we fixed a threshold value of 0.4 beyond which pixels were considered as positive for HES 130/0.4. In addition, a threshold value of 0.4 ensured that less than 1% of pixels were superior to this threshold in negative. In terms of color, positive pixels appeared in cyan-to-red while negative pixels in violet-to-blue. The comparison of two extracted spectra, one corresponding to a positive pixel (ratio = 0.9) and the other to a negative one (ratio = 0.2) (Fig 5), permitted to assess the intensity extent of the HES vibration compared to the tissue spectra. Other vibrations assigned to HES especially at 865 cm^{-1} were also visible but appeared superimposed to the tissue signal).

Later in our approach, we have determined for the set of the cases, the proportion of positive pixels (intensity ratio > 0.4) from Raman images collected on 10^3 μm^2 regions targeted tubular sections. Figure 4 depicted the color-coded Raman images (using the same ratio scale) for the four cases having received HES. For clarity, only one negative control was also displayed. The results of the pixels enumeration are indicated in Table 3. Firstly, a significant difference was highlighted between the HES-free controls and the tissues originating from patients who received HES. This result asserts the interest of Raman spectroscopy for HES detection in tissue samples; this benefice relies on the high specificity of the vibrational approach.

Secondly, an important variability appeared between the positive cases from 6% to 65%, for the percentage of pixels presenting an intensity ration over 0.4. Nevertheless, for each case, the percentage appeared higher than the mean+2SD percentage of positive pixels in negative controls (3.39%).

Discussion

Using Raman microspectroscopy (RM), a HES-specific Raman "fingerprint" was highlighted by comparing HES-incubated monocytes with sham monocytes, only incubated with 0.9% saline solution. Monocyte cells were chosen thanks to their ability to incorporate by phagocytosis macromolecules such as HES. Indeed HES is likely to remain present in monocyte lysosome after thorough rinsing the cell medium. The vibration at 480 cm^{-1}, assigned to a collective mode, permits to reveal the presence of HES macromolecule in biological material. This specific vibration serves as a basis signal to investigate the presence of HES in renal biopsies originated from patients with osmotic nephrosis and delayed recovery of renal function and who received HES 130/0.4 during collapse or donor resuscitation.

Hydroxyethyl starch (HES) is a synthetic colloid solution composed of modified natural polysaccharides and presents a structural similarity with glycogen which could accumulate in cells in pathologic conditions[27]. Unlike natural starches, HES is not rapidly hydrolyzed by circulating amylase and could persist longer in the intravascular compartments[28]. Since the 1970s, tissue accumulation of HES in rat experimental models has been reported [29] using a self-made antibody against HES [27]. Similar observations were reported in a pig model in acute hemodilution conditions with HES infusion (firsts generations of HES: 200/0.5, HES 100/0.5 or 200/0.62); and

the HES concentrations in various organs were measured 6 hours after HES administration. For these measurements, organ samples were frozen and homogenized in saline according to the method described by Appel et al. [30] , based on the the optical density of samples after several destructive biochemical steps. [31]. The authors reported that tissue storage of HES was higher in the kidney and liver than in other organs (lung, spleen, and lymph nodes) [31].More recently, tissue accumulation of high molecular weight HES (200/0.5 or 400/0.7) was reported in human patients by Sirtl *et al.* with a dose-dependent relation, in the skin, liver, small intestine, striated muscle and spleen. Using ultrastructural and immunoelectron microscopy with HES-specific monoclonal and polyclonal antibodies, the authors noted the persistence of HES accumulation in muscle tissue 16 months after HES infusion and in the skin 52 months after HES administration [12 32]. Concerning HES of lower molecular weight (130/0.4), it was detected in numerous organs or tissues like skin, liver, intestine or spleen and others human and animal models [33]. Alternatively, *Leuchner and al.* performed a radiolabelled HES detection to bring out HES tissue storage in rats [34]. Whatever their molecular weight, the current methods of detection of HES are based on immunohistochemical techniques usually by self-made antibody against HES or ultrastructural and immunoelectron microscopy. Nonetheless, to the best of our knowledge, Raman spectroscopy was used for the first time to detect HES 130/0.4 in a non-destructive label-free manner, with no need of specific tissue preparation. In addition, up to now, no study had investigated the accumulation of HES in human kidney biopsies. We are the firsts to report the persistent presence of HES in tubular cells of biopsy with proven osmotic nephrosis associated with HES 130/0.4 administration.

We underlined a variability in HES content ranging from 6% to 65% of positive pixels. Surprisingly, this variability was not associated with the clinical outcomes in

relation with the renal function. Indeed, the lower HES content was found in the patient with the absence of renal function recovery (case 2) whereas the higher HES content was found in the patient with the best renal function recovery (case 3). This variability could be explained by the volume and also by the flow rate of HES administration. Indeed, the HES quantity reabsorbed by tubular cells is certainly linked to the concentration of the molecule in the tubular lumen which depends on the total number of molecules infused, the infusion flow and the glomerular flow rate. According this hypothesis, the more the HES signal is intense, the higher absorption of HES by tubular cells resulting from a good tubular cells function at the moment of the infusion, without intrinsic renal injury. To validate this postulate, information on the quantity and flow of HES should be considered; data that are unfortunately not indicated in the current practice.

In our investigations, we were unable to show that HES could be detected in vacuolated tubular cells, since osmotic nephrosis cannot be recognized in the frozen samples (used for Raman microspectrosopy) but only in fixed and stained tissues. Osmotic nephrosis is characterized by a focal “clear-cell” transformation of proximal tubular epithelial cells showing isometric fine vacuolization of the cytoplasm. We also noticed that severely affected tubules were seen side by side with normal-appearance tubules. Brush borders were frequently well conserved. Morphological lesions were different from those observed after only ischemic kidney damage, where proximal tubules contain vacuoles of variable size accompanied by loss of brush border, bleb formation, and often desquamation of the epithelium from the basement membrane, and signs of regeneration[7]. In sucrose-induced osmotic nephrosis, it has been shown that the osmotic agent enters the tubular cells by means of pinocytosis,

and the pinocytic vacuoles subsequently fuse with each other and with lysosomes to form vacuoles that contain the indigestible agent (pinocytosis theory) [7,35]. This mechanism has been confirmed for several other molecules such as mannitol [36] or iodinated contrast media [37, 38]. This suggested pathway may be the same for HES-induced osmotic nephrosis, since HES is only slowly digestible by lysosomal enzymes, as shown by the development of acquired lysosomal storage disease in patients receiving large amounts of HES during chronic plasmapheresis [39]. We reported for the first time with Raman technique that HES could be stored for a long time in renal tubule supporting the "pinocytosis theory". Thus lysosomal alteration of tubular cells associated with HES accumulation may contribute to cell damage and could be the first step in the development of irreversible lesion, as also observed by drugs agencies (FDA, EMA) [11, 40, 41]. This process may prevent tubular regeneration that normally takes place after ischemia or sepsis induced tubular necrosis leading to irreversible kidney failure.

In our analysis, the regions of interest corresponding to renal tubules were selected by visual inspection of tissue cryosections without necessitating any staining. Since, these regions are homogenous in terms of tissue structures, it was not necessary to perform spectral histopathology (SHP) approach. SHP, based on multivariate statistical clustering of vibrational data collected at the microscopic scale, is efficient to recover the set of histological structures in complex various tissues such as articular cartilage [42], lung [43], skin [44, 45], or colon [46, 47]. This approach was detailed by Diem et al. in a review article, presenting various applications in the characterization of cancer tissues [48]. Contrary, in our study, a simple univariate method permitted to highlight the presence of HES in renal tubules; thanks to the 480 cm^{-1} vibration assigned to a collective mode of this macromolecule. This specific vibration, located in a spectral region where the tissue signal is of very low intensity,

authorized counting of HES positive pixels. This protocol was performed in the objective to demonstrate the presence of HES in kidney of patients who have received HES 130/0.4 solution for fluid resuscitation, without researching quantitative information about the accumulation of the product.

In addition to the detection of HES 130/0.4 in renal biopsies, Raman imaging, thanks to its high molecular specificity, could be used to detect other drugs which could be potentially toxic to kidney function. Advanced data processing such as SHP can be applied to exploit the spectral signal in case where markers distinctive of the drug are very subtle to be detected. Actually, means to detect drugs in tissue are limited, and required specific antibodies against each of these drugs which is complex and expensive protocols. Raman spectroscopy appears as a potential candidate technique, implementable in routine clinics, to detect in a label-free manner, the presence of exogenous molecules in tissues or organs like kidney.

Disclosure

All the authors declared no competing interests.

Acknowledgments: the authors acknowledge the Hematology department of the Reims University Hospital for supplying human blood for monocytes isolation.

REFERENCES

1. E. A. Hoste and J. A. Kellum, *Critical care medicine*, 2006, **34**, 2016-2017.
2. S. Uchino, J. A. Kellum, R. Bellomo, G. S. Doig, H. Morimatsu, S. Morgera, M. Schetz, I. Tan, C. Bouman, E. Macedo, N. Gibney, A. Tolwani and C. Ronco, *JAMA : the journal of the American Medical Association*, 2005, **294**, 813-818.
3. R. P. Dellinger, M. M. Levy, J. M. Carlet, J. Bion, M. M. Parker, R. Jaeschke, K. Reinhart, D. C. Angus, C. Brun-Buisson, R. Beale, T. Calandra, J. F. Dhainaut, H. Gerlach, M. Harvey, J. J. Marini, J. Marshall, M. Ranieri, G. Ramsay, J. Sevransky, B. T. Thompson, S. Townsend, J. S. Vender, J. L. Zimmerman and J. L. Vincent, *Intensive care medicine*, 2008, **34**, 17-60.
4. F. Schortgen, J. C. Lacherade, F. Bruneel, I. Cattaneo, F. Hemery, F. Lemaire and L. Brochard, *Lancet*, 2001, **357**, 911-916.
5. M. L. Cittanova, I. Leblanc, C. Legendre, C. Mouquet, B. Riou and P. Coriat, *Lancet*, 1996, **348**, 1620-1622.
6. F. M. Brunkhorst, C. Engel, F. Bloos, A. Meier-Hellmann, M. Ragaller, N. Weiler, O. Moerer, M. Gruendling, M. Oppert, S. Grond, D. Olthoff, U. Jaschinski, S. John, R. Rossaint, T. Welte, M. Schaefer, P. Kern, E. Kuhnt, M. Kiehntopf, C. Hartog, C. Natanson, M. Loeffler and K. Reinhart, *The New England journal of medicine*, 2008, **358**, 125-139.
7. M. Dickenmann, T. Oettl and M. J. Mihatsch, *American journal of kidney diseases : the official journal of the National Kidney Foundation*, 2008, **51**, 491-503.
8. A. Perner, N. Haase, A. B. Guttormsen, J. Tenhunen, G. Klemenzson, A. Aneman, K. R. Madsen, M. H. Moller, J. M. Elkjaer, L. M. Poulsen, A. Bendtsen, R. Winding, M. Steensen, P. Berezowicz, P. Soe-Jensen, M. Bestle, K. Strand, J. Wiis, J. O. White, K. J. Thornberg, L. Quist, J. Nielsen, L. H. Andersen, L. B. Holst, K. Thormar, A. L. Kjaeldgaard, M. L. Fabritius, F. Mondrup, F. C. Pott, T. P. Moller, P. Winkel and J. Wetterslev, *The New England journal of medicine*, 2012, **367**, 124-134.
9. J. A. Myburgh, S. Finfer, R. Bellomo, L. Billot, A. Cass, D. Gattas, P. Glass, J. Lipman, B. Liu, C. McArthur, S. McGuinness, D. Rajbhandari, C. B. Taylor and S. A. Webb, *The New England journal of medicine*, 2012, **367**, 1901-1911.
10. O. Bayer, K. Reinhart, Y. Sakr, B. Kabisch, M. Kohl, N. C. Riedemann, M. Bauer, U. Settmacher, K. Hekmat and C. S. Hartog, *Critical care medicine*, 2011, **39**, 1335-1342.
11. F. US Food and Drug Administration, Hydroxyethyl Starch Solutions: FDA Safety Communication - Boxed Warning on Increased Mortality and Severe Renal Injury and Risk of Bleeding, http://www.fda.gov/safety/medwatch/safetyinformation/safetyalertsforhumanmedicalproducts/ucm358349.htm, 2013).
12. C. Sirtl, H. Laubenthal, V. Zumtobel, D. Kraft and W. Jurecka, *British journal of anaesthesia*, 1999, **82**, 510-515.
13. H. P. Dienes, C. D. Gerharz, R. Wagner, M. Weber and H. D. John, *Journal of hepatology*, 1986, **3**, 223-227.
14. C. Krafft, *Analytical and bioanalytical chemistry*, 2004, **378**, 60-62.
15. J. R. Baena and B. Lendl, *Current opinion in chemical biology*, 2004, **8**, 534-539.
16. Z. Farhane, F. Bonnier, A. Casey and H. Byrne, *The Analyst*, 2015, DOI: 10.1039/c5an00256g.
17. J. Guo, W. Cai, B. Du, M. Qian and Z. Sun, *Biophysical chemistry*, 2009, **140**, 57-61.
18. L. Franzen, D. Selzer, J. Fluhr, U. F. Schaefer and M. Windbergs, *European journal of pharmaceutics and biopharmaceutics : official journal of Arbeitsgemeinschaft fur Pharmazeutische Verfahrenstechnik e.V*, 2012, DOI: 10.1016/j.ejpb.2012.11.017.
19. A. Tfayli, O. Piot, F. Pitre and M. Manfait, *European biophysics journal : EBJ*, 2007, **36**, 1049-1058.
20. S. Tfaili, C. Gobinet, G. Josse, J. F. Angiboust, A. Baillet, M. Manfait and O. Piot, *Analytical and bioanalytical chemistry*, 2012, DOI: 10.1007/s00216-012-6512-7.
21. A. Tfayli, E. Guillard, M. Manfait and A. Baillet-Guffroy, *The Analyst*, 2012, **137**, 5002-5010.

22. J. L. Suhalim, C. Y. Chung, M. B. Lilledahl, R. S. Lim, M. Levi, B. J. Tromberg and E. O. Potma, *Biophysical journal*, 2012, **102**, 1988-1995.
23. J. Lin, F. Lu, W. Zheng, S. Xu, D. Tai, H. Yu and Z. Huang, *Journal of biomedical optics*, 2011, **16**, 116024.
24. J. Shao, M. Lin, Y. Li, X. Li, J. Liu, J. Liang and H. Yao, *PloS one*, 2012, **7**, e48127.
25. A. Galat, *Acta biochimica Polonica*, 1980, **27**, 135-142.
26. R. Kizil, J. Irudayaraj and K. Seetharaman, *J Agric Food Chem.*, 2002, **50**, 3912-3918.
27. A. W. Richter and A. N. de Belder, *International archives of allergy and applied immunology*, 1976, **52**, 307-314.
28. J. C. Boon, F. Jesch, J. Ring and K. Messmer, *European surgical research. Europaische chirurgische Forschung. Recherches chirurgicales europeennes*, 1976, **8**, 497-503.
29. W. L. Thompson, T. Fukushima, R. B. Rutherford and R. P. Walton, *Surgery, gynecology & obstetrics*, 1970, **131**, 965-972.
30. W. Appel, V. Wirmer and D. Sprengard, *Zeitschrift fur klinische Chemie und klinische Biochemie*, 1968, **6**, 452-458.
31. C. Eisenbach, A. H. Schonfeld, N. Vogt, M. N. Wente, J. Encke, W. Stremmel, E. Martin, E. Pfenninger and M. A. Weigand, *Intensive care medicine*, 2007, **33**, 1637-1644.
32. S. Stander, Z. Szepfalusi, B. Bohle, H. Stander, D. Kraft, T. A. Luger and D. Metze, *Cell and tissue research*, 2001, **304**, 261-269.
33. R. Bellmann, C. Feistritzer and C. J. Wiedermann, *Clinical pharmacokinetics*, 2012, **51**, 225-236.
34. J. Leuschner, J. Opitz, A. Winkler, R. Scharpf and F. Bepperling, *Drugs in R&D*, 2003, **4**, 331-338.
35. S. L. Schwartz and C. B. Johnson, *Nephron*, 1971, **8**, 246-254.
36. A. B. Maunsbach, S. C. Madden and H. Latta, *Laboratory investigation; a journal of technical methods and pathology*, 1962, **11**, 421-432.
37. A. Nordby, K. E. Tvedt, J. Halgunset and O. A. Haugen, *Scanning microscopy*, 1990, **4**, 651-664; discussion 664-656.
38. P. Tervahartiala, L. Kivisaari, R. Kivisaari, I. Virtanen and C. G. Standertskjold-Nordenstam, *Investigative radiology*, 1991, **26**, 882-887.
39. J. J. Auwerda, F. W. Leebeek, J. H. Wilson, O. P. van Diggelen, K. H. Lam and P. Sonneveld, *Transfusion*, 2006, **46**, 1705-1711.
40. E. M. Agency, Hydroxyethyl-starch solutions (HES) should no longer be used in patients with sepsis or burn injuries or in critically ill patients – CMDh endorses PRAC recommendations, http://www.ema.europa.eu/ema/index.jsp?curl=pages/medicines/human/referrals/Hydroxyethyl_starch-containing_solutions/human_referral_prac_000012.jsp&mid=WC0b01ac05805c516f, 2013).
41. S. Mayor, *BMJ (Clinical research ed.)*, 2013, **347**, f6197.
42. A. Bonifacio, C. Beleites, F. Vittur, E. Marsich, S. Semeraro, S. Paoletti and V. Sergo, *Analyst.*, 2010, **135**, 3193-3204. doi: 3110.1039/c3190an00459f. Epub 02010 Oct 00422.
43. C. Krafft, D. Codrich, G. Pelizzo and V. Sergo, *Analyst.*, 2008, **133**, 361-371. doi: 310.1039/b712958k. Epub 712008 Jan 712914.
44. A. Nijssen, T. C. Bakker Schut, F. Heule, P. J. Caspers, D. P. Hayes, M. H. Neumann and G. J. Puppels, *J Invest Dermatol.*, 2002, **119**, 64-69.
45. C. Eklouh-Molinier, T. Happillon, N. Bouland, C. Fichel, M. D. Diebold, J. F. Angiboust, M. Manfait, S. Brassart-Pasco and O. Piot, *The Analyst*, 2015, **29**, 29.
46. C. Krafft, D. Codrich, G. Pelizzo and V. Sergo, *J Biophotonics.*, 2008, **1**, 154-169. doi: 110.1002/jbio.200710005.
47. J. Nallala, O. Piot, M. D. Diebold, C. Gobinet, O. Bouche, M. Manfait and G. D. Sockalingum, *Appl Spectrosc.*, 2014, **68**, 57-68. doi: 10.1366/1313-07170.
48. M. Diem, A. Mazur, K. Lenau, J. Schubert, B. Bird, M. Miljkovic, C. Krafft and J. Popp, *J Biophotonics.*, 2013, **6**, 855-886. doi: 810.1002/jbio.201300131. Epub 201302013 Nov 201300134.

Table 1: Clinical data of 4 patients with biopsy-proven osmotic nephrosis associated with HES 130/0.4 administration.

	Case 1	Case 2	Case 3	Case 4
Age	74	62	78	36 (D=38)
Sex	M	M	M	M (D=F)
Graft/NK	NK	NK	NK	Gaft
Baseline eGFR	88	85	unknow	D= 80
Type of AE	Septic shock	Septic shock	Septic shock	Cardiac arrest
To eGFR	0 (ARF)	0 (ARF)	0 (ARF)	0 (ARF)
To diuresis	500	400	0	0
eGFR at RB	RRT	RRT	30	41
Delay of RB	6 weeks	6 weeks	16 weeks	12 weeks
Histologic features on RB	ON-like and tubular necrosis injuries	ON-like and tubular necrosis injuries	ON-like injuries arteriosclerosis	ON-like injuries
M3 eGFR	32	RRT	40	41
M6 eGFR	25	RRT	30	45

Table 1 : Clinical data of 4 patients who received HES 130/0,5 (Voluven®). Age (years); M : Male; F : Female; NK : Native Kidney; D : Donnor; eGFR : Glomerular Filtration Rate estimated by MDRD equation (ml/min); AE : Acute Event; Diuresis (ml/24h); RB : Renal Biopsy ; ARF = Acute Renal Failure ; RRT : renal replacement therapy)

Table 2 : **Raman characterization of HES 130/0.4.** Band frequencies, band intensities and band assignment of Raman scattering spectrum of starch (s : strong, m : moderate, w : weak) [25] . Strong bands in bold.

Band frequency (cm^{-1})	Band intensity	Band Assignments
280	W	Different skeletal modes (collective vibration mode)
320	M	
360	M	
410	M	
480	**S**	
525	W	
580	M	Out-of-phase bending of hydrogen bonded hydroxyl groups
610	W	
715	M	
765	M	CH_2 rocking
865	**S**	C(1)-H(α) bending modes – water band C-O-C stretching
900	W	C(1)-H(β) bending modes
940	**S**	ring modes
1065	**S**	CH_2OH related modes
1085	**S**	COH deformation
1110	M	C-O-C antisymmetric bridge stretching
1125	M	C-O-C vibration
1150	M	COH stretching
1210	M	Antisymmetric in-plane ring stretching
1240	M	
1260	M	
1335	**S**	COH bending CH bending
1380	**S**	CH bending in-plane
1460	**S**	CH_2 bending in-plane

Table 3: Percentage area with an intensity ratio (480/1660 cm^{-1}) above the threshold value of 0.4. This threshold value for the ratio corresponded to the value below which less than 1% of pixels were positive in negative controls.

	Percentage area with intensity ratio (480/1660 cm^{-1}) >0.4
Case 1	15.63
Case 2	6.00
Case 3	65.00
Case 4	7.29
Average Cases ± SD	**23.48 ± 28**
Average Negative Controls ± SD	**0.87 ± 1.26***
Average Negative Controls + 2SD	**3.39***

* Comparison of the mean of cases vs the mean of negative controls using the Mann-Whitney Test (*p=0.004*).

SD, standard deviation.

Figure Legends

Figure 1: Raman spectra of starch (black) and HES 130/0.4 (red). The highest intensity peak is identified at 480 cm^{-1} in both spectra.

Figure 2: Principal Component Analysis (PCA) of Raman spectra of HES-incubated and sham monocytes. The score plot on the two first components shows a clear spectral discrimination of the HES-incubated and sham monocytes along PC1 (A). The first principal component (PC1) presents a high intensity region around 480 cm^{-1} (B).

Figure 3: Masson trichrome staining showing osmotic nephrosis injuries with vacuolated tubular cells (star) side by side with normal tubular sections (triangle)(x40) (A). Photo of a 10µm-thick frozen slide of the same renal biopsy dedicated to Raman acquisition, tubular sections with vacuolated cells cannot be detected on this photograph (B). (Scale bars: 25 µm)

Figure 4: Analysis by Raman spectroscopy of kidney biopsy with osmotic nephrosis lesions associated with HES 130/0.4. A spectral difference at the level of the vibration around 480 cm^{-1} is clearly visible between the two representative spectra as displayed in the inserts. (Scale bar: 25µm)

Panel A: Spectral image from case#2 built by intensity ratio (480/1660 cm^{-1}). Tubular sections are outlined with a dotted line. The color scale represents the intensity ratio: from violet (ratio=0) to red (ratio=1). Red areas on certain tubular sections can be highlighted while adjacent tubular sections appeared in violet or blue. Panel B: Raman spectra extracted from two points of the spectral image, corresponding to the blue area (♦) and red area (*).

Figure 5: Spectral images from the four cases: #1 (A) #2 (B) #3 (C) #4 5(D) and from a negative control (E). Spectral images from cases (A to D) present high intensity ratio while the negative control spectral image (E) is only composed of pixels with low intensity ratio similarly to other negative controls. (Scale bars 50µm)